Unique properties of magnetotransport in GaMnAs films grown on vicinal and high-index planes

2007 J. Phys.: Condens. Matter 19 165205

(http://iopscience.iop.org/0953-8984/19/16/165205)

IOP PUBLISHING JOURNAL OF PHYSICS: CONDENSED MATTER

J. Phys.: Condens. Matter **19** (2007) 165205 (19pp) doi:10.1088/0953-8984/19/16/165205

Unique properties of magnetotransport in GaMnAs films grown on vicinal and high-index planes

X Liu, J K Furdyna[1], M Dobrowolska, W L Lim, C Xie and Y J Cho

Department of Physics, University of Notre Dame, Notre Dame, IN 46556, USA

E-mail: xliu2@nd.edu and furdyna.1@nd.edu

Received 7 July 2006, in final form 19 September 2006
Published 6 April 2007
Online at stacks.iop.org/JPhysCM/19/165205

Abstract

Ferromagnetic III–Mn–V semiconductors such as GaMnAs represent systems in which electronic and magnetic properties are closely intertwined, which results in entirely new effects in electrical transport. We illustrate this by the unique and somewhat unexpected magnetotransport phenomena observed in GaMnAs films grown on vicinal substrates (i.e., on surfaces tilted by several degrees relative to the (100) plane) as well as on substrates with high-index-plane surfaces. In particular, it will be shown that such vicinal or high-index-plane GaMnAs layers manifest a striking asymmetry in the dependence of the planar Hall resistance R_{xy} on magnetic field, caused by the superposition of the planar Hall effect (PHE) and the anomalous Hall effect (AHE). This asymmetry is a direct manifestation of the effect of magnetocrystalline anisotropy in GaMnAs that confines the magnetization **M** to a preferred crystal plane *rather than to the plane of the film*, resulting in turn in a finite component of **M** normal to the sample plane. The ability to investigate PHE and AHE occurring simultaneously in the same sample revealed a clear relationship between the two effects, suggesting that PHE and AHE are fundamentally connected. The asymmetry of the resistance R_{xy} occurring in the PHE geometry in these GaMnAs layers also allows one to obtain *four* distinct zero-field resistance states that depend on the history of the experiment, making this effect of potential interest for building a unique *four-state* magnetic memory device. Moreover, measurements with the magnetic field normal to the growth plane in such tilted samples have revealed a new highly complex hysteresis behaviour of R_{xy}. These results, together with measurements of anisotropic magnetoresistance (AMR) measured on samples grown on high-index planes, point to the intimate relationship between magnetotransport and magnetocrystalline anisotropy in GaMnAs, providing new insights into this complex interdependence, as well as opening new opportunities for exploiting magnetic anisotropy for use in spintronic devices.

(Some figures in this article are in colour only in the electronic version)

[1] Author to whom any correspondence should be addressed.

1. Introduction

Ferromagnetic III–Mn–V semiconductors such as GaMnAs represent systems in which electronic and magnetic properties are closely intertwined, which results in entirely new effects in electrical transport. Striking examples of such interconnection are the planar Hall effect (PHE) and the anomalous Hall effect (AHE) which, through the interaction of charge carrier trajectories with the magnetization vector **M**, overshadow the normal Hall effect in ferromagnetic semiconductors. In this paper we will concentrate on these effects, as well as on the closely related anisotropic magnetoresistance, measured in special geometries that shed interesting new light on these phenomena and on magnetocrystalline anisotropy in III–Mn–V alloys generally.

Although there have been numerous experimental and theoretical studies of magnetotransport in GaMnAs and its nanostructures, most of these investigations have been limited to GaMnAs grown on (100) substrates [1–5]. Recently, however, the properties of GaMnAs layers grown on substrates other than (100) have also attracted considerable interest [6–12], since the study of these geometries offers important new insights into the magnetic properties and magnetization dynamics of ferromagnetic semiconductor films, and especially about the relation between magnetic anisotropy and lattice strain—an issue that may be crucial for future spintronic applications [13]. Here one should also note that the incorporation of Mn atoms and defects (e.g., As_{Ga}) depends on the substrate orientation. Thus the magnetic parameters—such as the all-important orientation of the easy axis of magnetization **M**—may be quite different in GaMnAs grown on these 'tilted' orientations from those found in GaMnAs layers grown on the conventional (100) surfaces.

Successful deposition of high-quality GaMnAs layers has been demonstrated on vicinal substrates (with the growth plane tilted by several degrees from the (100) plane) [10, 11], and on GaAs substrates with the following high-index planes: (411)A [6], (311)A [7, 12] and (311)B [7]. Various magnetization, magnetotransport and ferromagnetic resonance measurements [14] have also been carried out on such layers in order to understand the complex magnetic properties of GaMnAs films with these new orientations. An especially important feature in such films is that in these nonstandard orientations there occurs a competition between the strain-induced uniaxial anisotropy associated with the growth direction and the cubic anisotropy defined by the principal cubic axes (which, unlike the case of specimens grown on the (100) substrates, are now tilted out of the sample plane). It will be show that these new orientations open prospects for new interesting magnetotransport features in GaMnAs—and, by extension, in other ferromagnetic III–Mn–V alloys as well.

In this paper we will use measurements of the Hall resistance R_{xy} obtained with the magnetic field applied in the layer plane at various angles relative to the current as a means of comparing the properties of in-plane magnetization in GaMnAs epilayers grown on standard (100), on vicinal (slightly tilted relative to (100)) GaAs substrates, and on high-index ((511) and (311)) GaAs substrates. We should note here that the PHE exists in these geometries regardless of substrate orientation. The anomalous Hall effect (AHE) contribution, on the other hand, arises only due to the presence of a projection of the magnetization normal to the sample surface, an effect that is induced by cubic magnetocrystalline anisotropy forcing the magnetization **M** to lie along a preferred crystal direction rather than along the plane of the film. Thus the AHE contribution to R_{xy} measured in the PHE geometry is only present in GaMnAs samples grown on substrates other than (100).

The emphasis in this paper will be on measurements in the PHE geometry, because of the rather striking new effects which are observed in this geometry, and which include interesting prospects for novel magnetic memory devices. For completeness, however, we will also explore

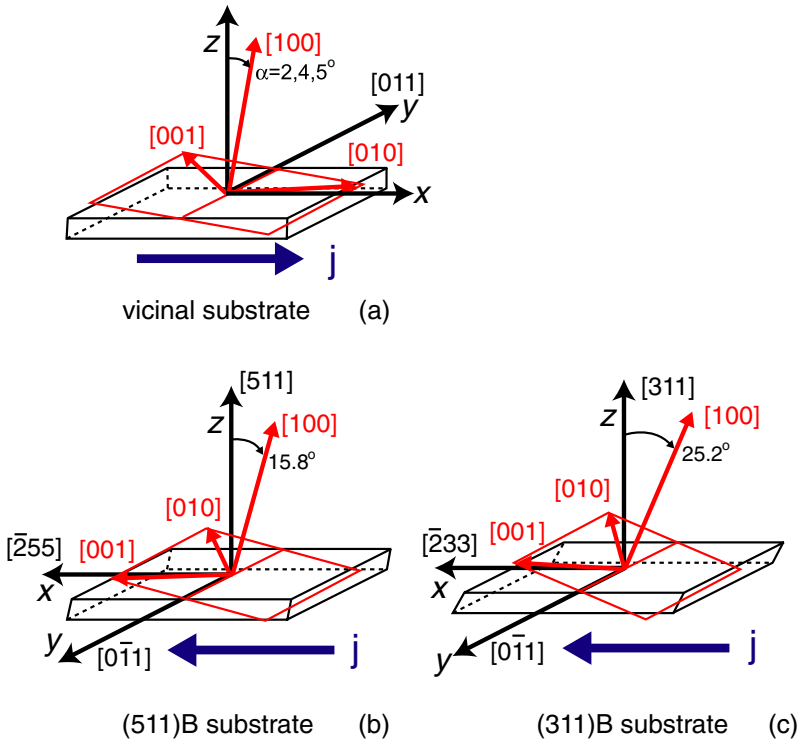

Figure 1. Sample geometry and orientation of the crystallographic directions for GaMnAs layers grown (a) on a vicinal GaAs substrate; (b) on a (511)B GaAs substrate; and (c) on a (311)B GaAs substrate.

in considerable depth the properties of the AHE and of anisotropic magnetoresistance (AMR) in these nonstandard geometries which, together with the PHE, offer valuable new insights into the interplay of the magnetization and electronic transport in ferromagnetic semiconductors.

2. Sample fabrication and experimental procedure

To study the effects described above we have fabricated two series of specimens by low-temperature molecular beam epitaxy (MBE) using a RIBER 32 R&D MBE system, as follows. For vicinal samples, GaMnAs layers were grown with the thickness of 46 nm on vicinal semi-insulating GaAs substrates with three different tilts, along with a control sample grown on a standard (100) substrate. The planes of the vicinal substrates were tilted by 2°, 4° and 5° away from the (100) plane, with the tilt angle α measured from the (100) plane toward the (1$\bar{1}$1)B plane. This geometry is shown in figure 1, along with schematic diagrams for samples grown on the (511) and (311) surfaces, including coordinate axes for all configurations. For vicinal growths all substrates—the three vicinal orientations and the (100) control substrate—were placed side-by-side on the molybdenum block, and the MBE deposition of all four samples was carried out simultaneously to assure the same growth conditions in all samples. For the high-index plane series, 48 nm layers of GaMnAs were grown on four high-index semi-insulating GaAs substrates with different orientations (i.e., (511)A, (511)B, (311)A, and (311)B), along with 'companion' control sample grown on a standard (100) substrate. As in the case of the vicinal specimens, the substrates were placed side-by-side on the growth stage and the

deposition of the high-index plane series was carried out simultaneously to assure identical growth conditions. The growth surface was monitored by reflection high-energy electron diffraction (RHEED), which showed a streaky pattern throughout the growth, indicating that the growth proceeded epitaxially.

All as-grown GaMnAs films used in this study exhibit ferromagnetism up to a transition temperature $T_C \sim 60$ K, as determined by SQUID measurements. In order to determine the degree of lattice strain, both the symmetric and asymmetric x-ray diffraction (XRD) measurements were carried out by reflection from several planes using a double-crystal x-ray diffractometer with Cu Kα_1 radiation. The concentrations of Mn were estimated from measurements on the reference GaMnAs(100) films grown alongside the tilted layers, and were 7% for the vicinal series and 5% for the high-index series.

The samples described above were characterized by magnetotransport measurements using a five-probe Hall geometry with indium ohmic contacts. The epilayers were patterned into 50 μm $\times$ 250 μm Hall bars by photolithography, with the long axis oriented along the $[01\bar{1}]$ for the vicinal samples; and along $[\bar{2}33]$ and $[\bar{2}55]$ directions for the samples grown on (311) and (511) substrates, respectively. In discussing the magnetotransport measurements carried out on the vicinal and high-index layers, it is important to distinguish between the morphological sample plane (i.e., the measuring plane) and the (100) crystal plane. As shown in figure 1, to make that distinction we will use the coordinates x, y, z when referring to the macroscopic morphology of the layer, z being the direction normal to the layer surface, x the direction of the current flow, and y the direction of the Hall voltage. Magnetotransport discussed in this paper will involve the Hall resistance R_{xy} measured in two field geometries: with field **H** applied in the plane of the sample (the xy plane) at an arbitrary azimuthal angle φ_H, which for convenience we will continue to call the PHE geometry, even though in vicinal and high-index samples there is an essential AHE contribution in this configuration; and with **H** applied normal to the film (**H** $\parallel z$), which we will refer to as the AHE geometry.

3. Results and discussion

3.1. Magnetotransport results on vicinal GaMnAs films

3.1.1. The planar and anomalous Hall effects. To investigate the effect of the tilt of the sample plane on magnetotransport in GaMnAs, we begin with measurements in the PHE and AHE geometries. Figure 2 shows the R_{xy} signal measured at 4.2 K in these two geometries on samples with vicinal angles of 0°, 2° and 5°. A striking feature is observed in the AHE geometry: as the vicinal angle increases, we see clearly a gradual emergence and increase of the hysteresis loop around $H \sim 0$ (a feature absent in the reference non-vicinal sample). Since the presence of a low-field hysteresis loop in the AHE requires the presence of a component of **M** perpendicular to the sample plane, this result indicates that a finite component M_z exists in the vicinal samples, and that it increases with the tilt angle. Simultaneously, in the PHE geometry we observe a striking difference between the behaviours of R_{xy} in normal and vicinal samples. Specifically, the values of the Hall resistance plateaus (which correspond to the intermediate magnetization states in the process of magnetization reversal) are conspicuously unequal in vicinal samples. To explain this asymmetry, it is of key importance to note that when **M** is confined by magnetocrystalline anisotropy to one of the easy axes ([001] or [010]) in the (100) plane, in vicinal samples there will exist a nonzero component of magnetization M_z normal to the sample plane (consistent with the observation of hysteresis loops in the AHE described above). The results in figure 2 show that the films grown on vicinal substrates provide an ideal opportunity to separate the contributions of shape and crystalline anisotropy, since in the vicinal

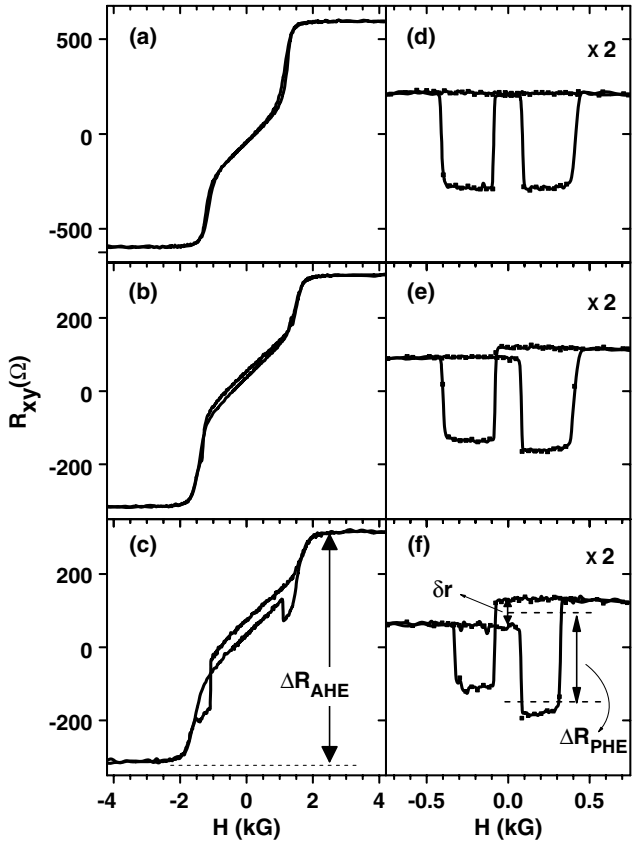

Figure 2. Hall resistances R_{xy} observed in the AHE (left panel) and PHE (right panel, at $\varphi_{\mathrm{H}} = 102°$) geometries for samples grown on vicinal substrates with ((a), (d)) $\alpha = 0°$, ((b), (e)) $\alpha = 2°$, and ((c), (f)) $\alpha = 5°$ vicinal angles.

geometry the principal crystal axes no longer lie in the sample plane. In particular, our results in this series of vicinally grown GaMnAs films conclude that the orientation of the easy axis is determined primarily by the magnetic crystalline anisotropy.

We recall that the PHE contribution to R_{xy} observed in the PHE geometry is given by the function $(R_{\parallel} - R_{\perp})\sin(2\varphi)$, where $R_{\parallel}$ and $R_{\perp}$ are resistances corresponding to in-plane **M** orientations parallel and normal to the current **I**, respectively; and the *sign* of the AHE contribution to R_{xy} is determined by the *sign* of M_z. The asymmetry of R_{xy} observed in the present measurement can therefore be explained as the vector sum of the AHE and PHE contributions. This is illustrated by figure 3: depending on the direction of the in-plane component of magnetization **M** (along the four easy axes: [010], [001], [0$\bar{1}$0] and [00$\bar{1}$]), there are *four different combinations* of PHE and AHE contributions to R_{xy} when $R_{\parallel} < R_{\perp}$: for **M** $\parallel$ [010], both the PHE and AHE are negative, i.e., PHE($-$), AHE($-$); for **M** $\parallel$ [001] we have PHE($+$), AHE($+$); for **M** $\parallel$ [0$\bar{1}$0] we have the combination PHE($-$), AHE($+$); and for **M** $\parallel$ [00$\bar{1}$] we have PHE($+$), AHE($-$). As a result, during the magnetization reversal process, the magnetization **M** will go through all these four states in some specific sequence (depending both on the history and on the orientation of the applied magnetic field), which will lead to the asymmetric shift of R_{xy} observed in the PHE geometry as shown in figure 2.

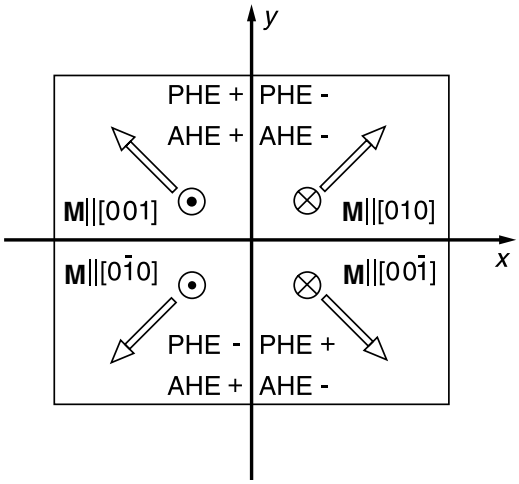

Figure 3. PHE and AHE contributions to Hall resistances R_{xy} measured in the PHE geometry for four easy axes of magnetization **M** constrained to the (100) plane in samples grown on vicinal substrates.

In order to confirm the above conjecture, we turn to the relation between the asymmetric shift of R_{xy} observed in the PHE geometry and the value of R_{xy} measured in the AHE geometry. In the AHE geometry the magnitude of R_{xy} will saturate when the field is sufficiently strong to turn the full magnetization of the sample **M** normal to the layer plane. In our samples this occurs above 2.0 kOe, as seen from the saturation of R_{xy} in figure 2 (left panels). Since the value of R_{xy} at saturation (which we will indicate by $\Delta R_{\rm PHE}$, as shown in figure 2) is caused by the full magnetization $M_{\rm sat}$, and the asymmetric shift of R_{xy} observed in the PHE geometry at $H \sim 0$ in vicinal samples (indicated by δr in the figure) results from the AHE contribution caused by the projection M_z, we can write $\delta r/\Delta R_{\rm AHE} = M_z/M_{\rm sat}$. Furthermore, when **M** at low fields is along one of the easy axes in the (100) plane, its projection normal to the sample plane is given by

$$\frac{M_z}{M_{\rm sat}} = \gamma \sin\alpha = \frac{\delta r}{\Delta R_{\rm AHE}}, \tag{1}$$

where α is the tilt angle of the vicinal plane with respect to (100). The value of the factor $\gamma = \cos\frac{\pi}{4} = \frac{\sqrt{2}}{2}$ arises because the easy axis of **M** is along either the [010] or the [001] direction at low temperatures, and the tilt angle of the substrate is in the (011) plane. In figure 4(a) we plot $\delta r/\Delta R_{\rm AHE}$ for the vicinal angles 0°, 2°, 4°, and 5°. The striking agreement of the data with (1) provides compelling evidence that at low fields the magnetization **M** is confined to one of the easy axes in the (100) crystal plane (presumably by the well established cubic and uniaxial magnetocrystalline anisotropy in thin GaMnAs films), which in vicinal samples results in a nonzero component M_z normal to the sample plane.

In the course of our analysis of the asymmetric shift δr in R_{xy} measured in the PHE geometry we observe that the ratio of δr to the average jump in R_{xy} denoted as $\Delta R_{\rm PHE}$ in the right panel of figure 2(c) also increases linearly with the vicinal angle α. Note that the quantity $\Delta R_{\rm PHE}$ marked in figure 2(c) corresponds to the jump in R_{xy} *without* the AHE contribution. This relation is shown by the dashed–dotted plot of $\delta r/\Delta R_{\rm PHE}$ in figure 4(b). The simultaneous observation that $\delta r/\Delta R_{\rm AHE}$ (figure 4(a)) and $\delta r/\Delta R_{\rm PHE}$ (figure 4(b)) both vary linearly with α suggests that there exists a relationship between $\Delta R_{\rm AHE}$ and $\Delta R_{\rm PHE}$: $\Delta R_{\rm AHE} = c\Delta R_{\rm PHE}$,

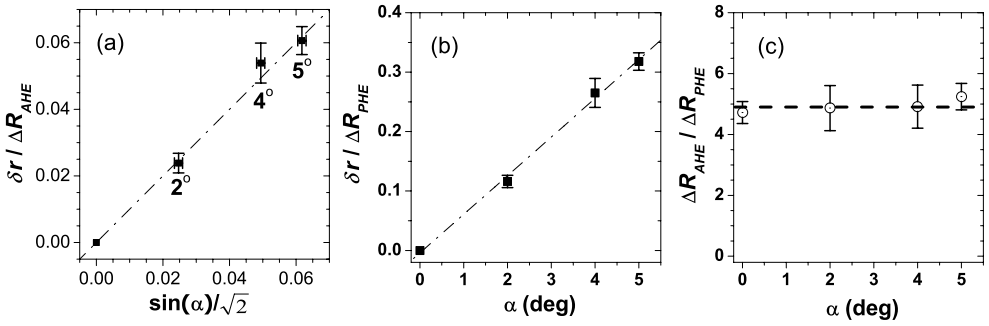

Figure 4. Vicinal angular dependences of (a) the ratio $\delta r/\Delta R_{\rm AHE}$, (b) $\delta r/\Delta R_{\rm PHE}$, and (c) $\Delta R_{\rm AHE}/\Delta R_{\rm PHE}$, demonstrating a linear relationship between $\Delta R_{\rm AHE}$ and $\Delta R_{\rm PHE}$. The dotted and dashed lines are guides for the eye.

where $c = 4.9 \pm 0.8$ is a proportionality constant *that is independent* of the applied fields, field angles, and of the vicinal angles, as shown in figure 4(c). This relationship is quite surprising, because the AHE is understood as arising from the form of carrier scattering in a ferromagnet (skew or side-jump) [15], while the PHE is fundamentally a manifestation of AMR [16], with no obvious connection between the two mechanisms. Thus, although in the context of the present paper the observation of the relationship of the AHE and the PHE is only a phenomenological by-product of the investigation of R_{xy} in vicinal GaMnAs layers, further study of this relationship may shed valuable light on the underlying physics of both effects. In particular, since it is reasonable to expect that the constant c connecting the two effects depends on the hole and the Mn concentrations, it should be especially interesting to extend such study measurements on samples with other values of these parameters in order to shed further light on this unexpected but possibly important result.

In addition to its fundamental meaning, the fact that $\Delta R_{\rm AHE}/\Delta R_{\rm PHE}$ is a constant also provides compelling support for the single-domain assumption which we use in interpreting our results. This can be argued as follows. The value of $\Delta R_{\rm AHE}$ is obtained from the saturation region of the AHE indicated in figure 2, i.e., when the magnetic field is strong enough to align *all* the magnetic moments normal to the sample plane, so that the sample is a single domain. The fact that the ratio $\Delta R_{\rm AHE}/\Delta R_{\rm PHE}$ is a constant then indicates that the measured contribution to the PHE is also made by the entire (i.e., single) domain. The same conclusion can be drawn from the linearity of $\delta r/\Delta R_{\rm AHE}$. This is not at all surprising, since in GaMnAs/GaAs specimens the domains are typically quite large [17].

3.1.2. Temperature dependence of the PHE asymmetry in vicinal GaMnAs films. We note parenthetically that at low temperatures (about 4.2 K) in all our GaMnAs samples, the easy axis of magnetization is along one of the crystallographically equivalent [010] and [001] directions in the (100) plane, consistent with the observations reported by Welp *et al* [17]. However, it is well known that the easy axis can change from [010] or [001] to the $[0\bar{1}1]$ orientation as the temperature is increased [18–20]. As shown in figure 5, we have indeed observed interesting changes in the behaviour of R_{xy} in our vicinal GaMnAs samples at higher temperatures, that we ascribe to an in-plane switching of the easy axes.

As an example, figure 5 shows the hysteresis in R_{xy} in the PHE geometry at a fixed field angle $\varphi_{\rm H} = 172°$, observed by reversing the field between $+1.0$ and -1.0 kOe at a series of temperatures. The form of the resistance 'jumps' becomes much more complicated as the temperature T is increased. In particular, we see in figure 5 two distinctly different trends in

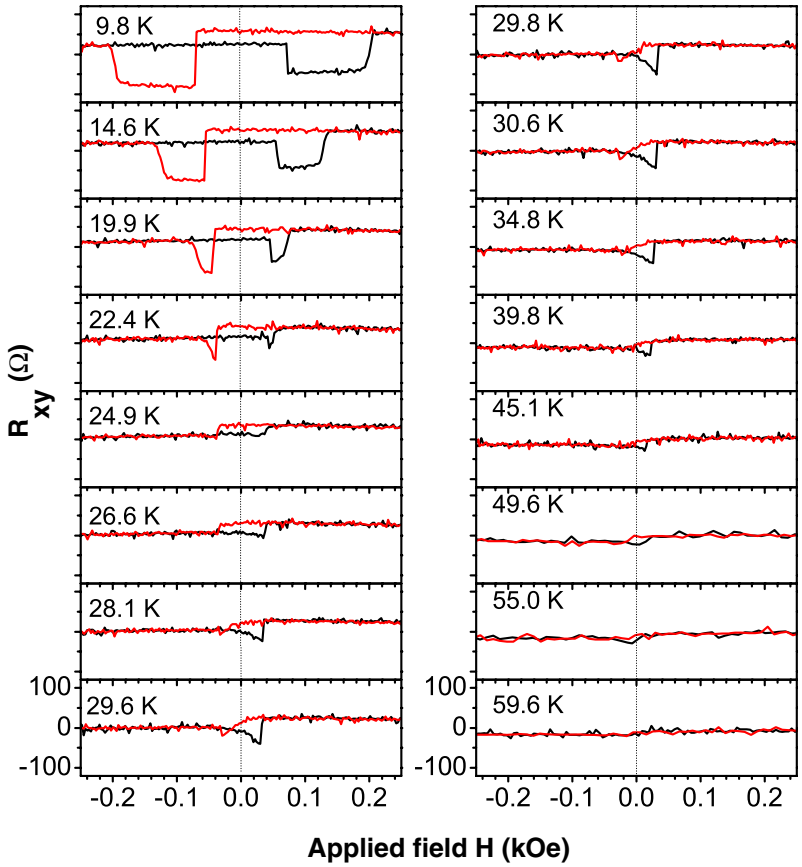

Figure 5. Magnetic field dependence of Hall resistance R_{xy} observed for a GaMnAs sample grown on a vicinal substrate with a 5° tilt relative to the (100) plane, measured in the PHE geometry at $\varphi_{\mathrm{H}} = 172°$ at a series of temperatures.

the behaviour of R_{xy} on either side of $T \approx 24.9$ K, where a square-like hysteresis loop first appears. Below 24.9 K the asymmetric shift in resistance plateaus decreases in amplitude as the magnetization gets weaker with the increase of temperature. At the same time, the widths of resistance plateaus rapidly shrink as the temperature increases, and eventually disappear at about 24.9 K, signalling a transition into a different behaviour. Above that temperature the asymmetric resistance peaks (but no longer in the form of asymmetric plateaus) reappear in the value of R_{xy}. As shown in figure 5, unlike those wide and sharp planar Hall resistance jumps at low temperatures, there are now only two jumps, each preceded by a slowly evolving downward slope. Furthermore, the jumps are strikingly unequal in the two field orientations: the jump seen on the positive field side is quite obvious, while the jump on the negative field side is barely distinguishable from the noise. The asymmetry between the two jumps peaks at about 30 K, and the entire effect gradually diminishes with increasing temperature, vanishing completely above $T \approx 45$ K.

In figure 6(a), we zoom in on the characteristic features of R_{xy} at four different temperatures to emphasize the trends described above. Here one should note that, as the temperature increases, the cubic anisotropy will decrease, and this will result in the change of the easy axis orientation from [010] and [001] to the [01$\bar{1}$] direction. It is instructive to discuss

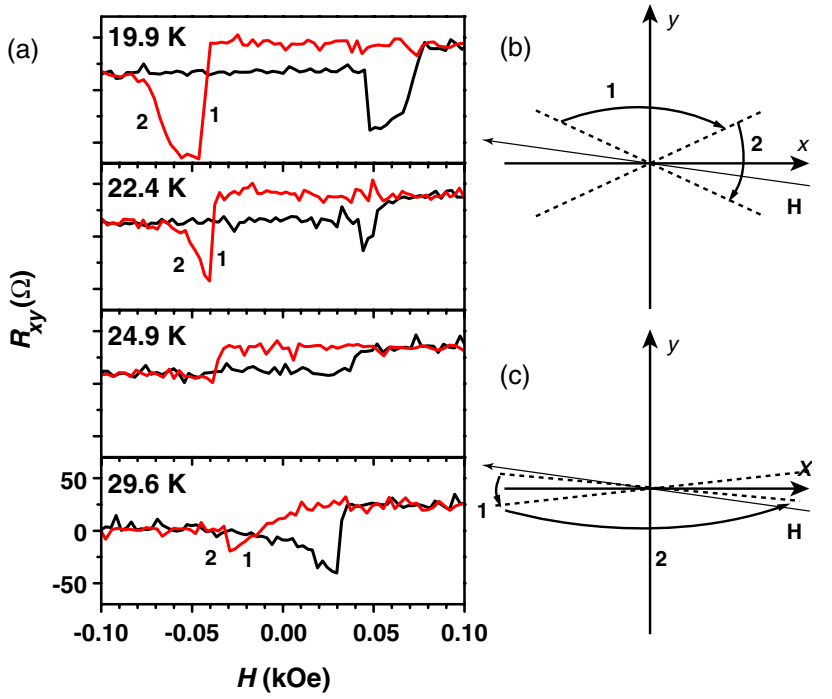

Figure 6. (a) Magnetic field dependence of Hall resistance R_{xy} observed in the PHE geometry for a GaMnAs sample grown on a vicinal substrates with a 5° tilt angle, measured at four temperatures at $\varphi_H = 172°$. The specific temperatures are chosen to illustrate special features that emerge in R_{xy} as the temperature increases. (b) Schematic diagram of spin switchings at a low temperature. (c) Schematic diagram of spin switchings at a high temperature. The dashed lines in (b) and (c) represent the easy axes of magnetization.

the effect of this change on the process of magnetization reversal. At low temperatures, the easy axes of magnetization are close to the [001] and [010] directions, as shown in figure 6(b). In this situation (e.g., at $T = 19.9$ and 22.4 K in figure 6) the magnetization reversal can be described by two spin switchings, marked (1) and (2) in figure 6(b). As the temperature increases, spin switching (2) evolves into a continuous (rather than abrupt) multi-domain process, while spin switching (1) is always an abrupt ∼90° domain rotation. As the temperature continues to increase, eventually the easy axes will approach the $[01\bar{1}]$ direction. In this situation (e.g., at $T = 29.6$ K in figure 6), the magnetization reversal process can be described by a two-spin switching (1) and (2) shown in figure 6(c). However, here spin switching marked (1) is a multi-domain process, while the spin switching (2) is an abrupt ∼180° domain reorientation. Between these two situations (at about $T = 24.9$ K in figure 6), while the easy axis is now nearly parallel to the magnetic field orientation, magnetization reversal occurs essentially along the magnetic field, and consequently the PHE jump vanishes. The square hysteresis loop seen in the Hall measurement R_{xy} at that temperature is thus a pure AHE signal induced by M_z.

Thus the temperature dependence of R_{xy} seen in figure 5 arises because the easy axis of magnetization reorients from [010] direction to the $[01\bar{1}]$ direction, presumably due to the increasing role of the uniaxial anisotropy in the (100) plane as the cubic anisotropy become less dominant with increasing temperature. Such temperature-induced transformation from [010] to $[01\bar{1}]$ easy axes has been seen very clearly in, for example, domain imaging experiments of Welp *et al* [17]. On the other hand, the enhancement of the asymmetric shift (seen already at

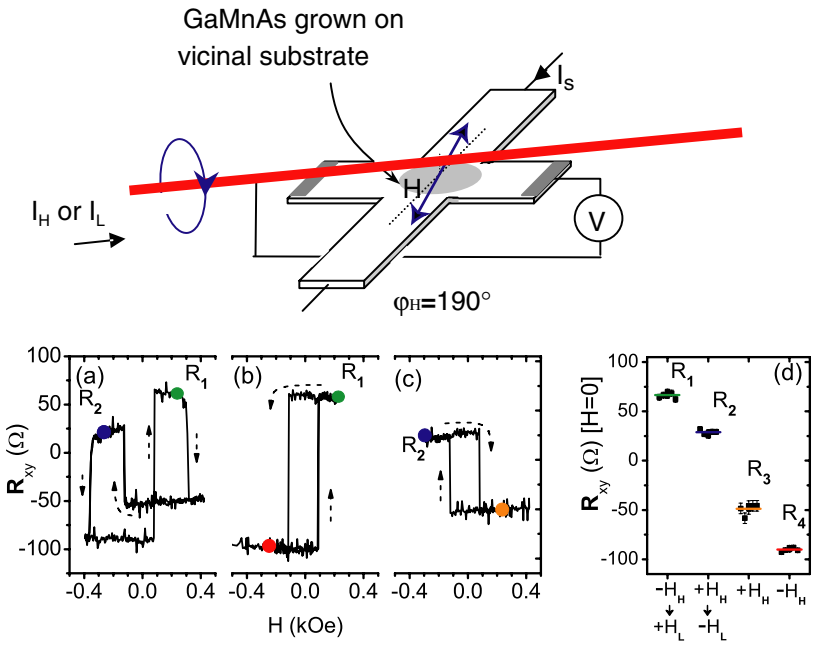

Figure 7. Top: A conceptual device utilizing a single conducting wire that could carry a higher current $\pm I_{\rm H}$ or a lower current $\pm I_{\rm L}$, which can be used to define the field strength **H** at the centre of the cross. Here, $I_{\rm H}$ and $I_{\rm L}$ function as the sequential inputs that will lead to one of four 'memory' resistance states detected by the transverse Hall voltage V at zero field. Is is the base current flowing through the device. Bottom: Resistances R_{xy} observed in the PHE geometry at $\varphi_{\rm H} = 190°$ for a complete field sweep loop (a) from -2.0 kOe $\rightarrow +2.0$ kOe $\rightarrow -2.0$ kOe; (b) from -2.0 kOe $\rightarrow +0.2$ kOe $\rightarrow -2.0$ kOe; and (c) from $+2.0$ kOe $\rightarrow -0.2$ kOe $\rightarrow +2.0$ kOe. (d) Demonstration of nonvolatile memory states at $\varphi_{\rm H} = 190°$ for the four values of R_{xy} ($R_1 = +66\ \Omega$, $R_2 = +29\ \Omega$, $R_3 = -49\ \Omega$ and $R_4 = +90\ \Omega$) obtained by applying $H_{\rm H}$ (2.0 kOe) and $H_{\rm L}$ (0.2 kOe) in the PHE geometry in specific sequences before switching off the field.

30 K) can probably be attributed to an increase of the factor γ in (1), which is approaching *unity* because we now have the easy axis of **M** along $[01\bar{1}]$, instead of the [010] or [001] directions.

3.1.3. Vicinal GaMnAs layers as a four-valued magnetic memory device. The above results clearly demonstrate that in GaMnAs films it is the magnetocrystalline anisotropy rather than shape anisotropy that establishes the preferred direction along which the magnetization **M** tends to align. In addition to this conclusion, the observations reported in this paper also point to the possibility of a four-state magnetic memory device which can be operated by applying a specific sequence of magnetic fields to a vicinal sample, as shown in figure 7. We demonstrate the idea of such a device using the sample with a vicinal angle of 5°. As shown in figure 7, using two field strengths, $H_{\rm H} = 2$ kOe and $H_{\rm L} = 0.2$ kOe applied at $\varphi_{\rm H} = 190°$, it is possible to retain any of four different resistance states R_{xy} at $H = 0$, depending on the sequence in which these fields are applied before the field is switched off. For example, referring to the data shown in figure 7(d),

- applying a positive $H_{\rm H}$ and switching it off results in $R_{xy} = -49\ \Omega$;
- applying a negative $H_{\rm H}$ gives $R_{xy} = -90\ \Omega$ after the field is switched off;

- applying a sequence of $-H_{\mathrm{H}}$ followed by $+H_{\mathrm{L}}$ and then switching off the field results in $R_{xy} = +66\ \Omega$;
- applying a sequence of H_{H}, $-H_{\mathrm{L}}$ results in $R_{xy} = +29\ \Omega$ after the field is switched off.

Although for a given sample the values of the four resistance states R_{xy} illustrated in figure 7 do not depend on the azimuthal angle of the applied field φ_{H}, the angle φ_{H} does determine the sequence of the fields required to obtain any of these states at zero field. Since the resistance states can be reversed upon crossing the hard axis, it is then possible to use two in-plane orthogonal fields as two logic inputs to set the actual field angle in any half-quadrant between the easy axes [010] and [001]. This will rearrange the sequential field operations required for reaching each of the resistance states. Such controls could resemble a magneto-logic device [21], or a reconfigurable nonvolatile four-state magnetoresistance random access memory (MRAM) with a double capacity, as well as additional opportunities for manipulation. Based on this, we propose a simple (proof of concept) memory device depicted in figure 7. As shown in the figure, a single conducting wire which could carry a stronger current I_{H} and a weaker current I_{L} can be used to define the direction of the field **H** at the centre of the Hall bar. These two currents can then act as sequential inputs, while the planar Hall voltage becomes the output. In this way the device can function as a four-state memory or logic device, as described in the preceding paragraphs.

3.2. Magnetotransport in GaMnAs films grown on high-index substrates

The results presented above were obtained on vicinal GaMnAs layers grown on substrate surfaces with relatively small tilt angles α relative to the (100) cubic plane. As the vicinal angle increases, eventually we will approach one of the standard high-index planes. For example, for $\alpha = 54.7°$ the 'vicinal' sample surface would coincide with the (111) plane. It is therefore interesting to extend the study of magnetotransport already described to such high-index planes, which correspond to much larger tilts relative to the cubic axes, but which also have distinct symmetries associated with the specific plane orientations, which affect epitaxy, strain, and other physical properties in unique ways. For this study we have chosen GaMnAs films grown on the (311) and (511) planes since, in addition to their high Miller indices, these planes are also polar, with distinct properties characteristic of As- and Ga-rich surfaces (denoted as, e.g., (311)A and (311)B surfaces, respectively), that affect the growth; and this should have additional effects on the magnetic properties of GaMnAs deposited on such surfaces.

3.2.1. Strain and magnetic anisotropy in high-index-plane GaMnAs layers. Typical results of symmetric and asymmetric XRD measurements are shown in figure 8 for GaMnAs layers grown on high-index substrates. The $\theta/2\theta$ scans for symmetric (311) and (511) Bragg reflections have been measured with four different azimuth angles of the incident beam by rotating the GaMnAs films grown on (311)B and (511)B GaAs substrates counterclockwise in four 90° steps about the [311] or the [511] directions, respectively. The fact that all four scans lie exactly on top of each other indicates that the growth plane of each GaMnAs layer was kept parallel to the surface of the substrate on which it was grown. Importantly, from the $\theta/2\theta$ scans the lattice distortion $\Delta d/d$, defined as the relative change of the distance between the lattice plains, reveals the existence of a compressive strain in GaMnAs layers grown on the high-index GaAs substrates. In addition, the existence of a compressive strain in the GaMnAs layer plane is also clearly seen from the difference in the peak positions relative to the GaAs substrate between the high and low incident angle configurations for the asymmetric XRD scans of the (400) reflection. It is important to note that, in contrast to vicinal layers, where the strain was essentially that characteristic of the (100) plane due to the large (100) terraces on which the

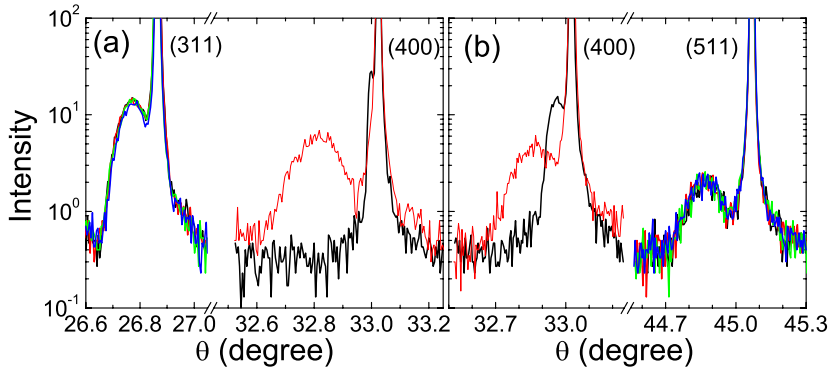

Figure 8. Symmetric and asymmetric x-ray diffraction curves for GaMnAs grown on (a) (311)B and (b) (511)B substrates. The results show that GaMnAs layer is strained along [311] or [511] directions for the (311)B or (511)B substrates, respectively. The symmetric x-ray diffraction (311) and (511) was measured each with four different azimuth angles of the incident beam; and asymmetric x-ray diffraction (400) was measured at high incident angle (heavy, black curve) and low incident angle (light, red curve). In panel (a), for the (400) reflection measured at high incident angle the peaks from GaMnAs and from the GaAs substrate are coincident with one another.

growth actually occurred, now the XRD results indicate that the strain is characteristic of the specific high-index planes, i.e., the (511) or the (311) plane.

Based on the XRD results, we therefore propose that the magnetic anisotropy of GaMnAs grown on high-index GaAs substrates can be parameterized into a cubic magnetic anisotropy along ⟨100⟩ axes and an additional uniaxial anisotropy along the growth direction (i.e., [311] or [511], respectively). For GaMnAs grown on (311) GaAs substrates this will lead to the free energy density

$$\begin{aligned} F = &-MH\left[\cos\theta\cos\theta_{\mathrm{H}} + \sin\theta\sin\theta_{\mathrm{H}}\cos\left(\varphi-\varphi_{\mathrm{H}}\right)\right] - K_{\mathrm{eff}}\cos^2\theta \\ &- \frac{1}{2}K_4\left[\left(\frac{3}{\sqrt{22}}\sin\theta\cos\varphi + \frac{1}{\sqrt{2}}\sin\theta\sin\varphi + \frac{1}{\sqrt{11}}\cos\theta\right)^4\right. \\ &+ \left(\frac{3}{\sqrt{22}}\sin\theta\cos\varphi - \frac{1}{\sqrt{2}}\sin\theta\sin\varphi + \frac{1}{\sqrt{11}}\cos\theta\right)^4 \\ &+ \left.\left(-\sqrt{\frac{2}{11}}\sin\theta\cos\varphi + \frac{3}{\sqrt{11}}\cos\theta\right)^4\right]; \end{aligned} \tag{2}$$

and for GaMnAs grown on (511) GaAs substrates to

$$\begin{aligned} F = &-MH\left[\cos\theta\cos\theta_{\mathrm{H}} + \sin\theta\sin\theta_{\mathrm{H}}\cos\left(\varphi-\varphi_{\mathrm{H}}\right)\right] - K_{\mathrm{eff}}\cos^2\theta \\ &- \frac{1}{2}K_4\left[\left(\frac{5}{3\sqrt{6}}\sin\theta\cos\varphi + \frac{1}{\sqrt{2}}\sin\theta\sin\varphi + \frac{1}{3\sqrt{3}}\cos\theta\right)^4\right. \\ &+ \left(\frac{5}{3\sqrt{6}}\sin\theta\cos\varphi - \frac{1}{\sqrt{2}}\sin\theta\sin\varphi + \frac{1}{3\sqrt{3}}\cos\theta\right)^4 \\ &+ \left.\left(-\frac{\sqrt{2}}{3\sqrt{3}}\sin\theta\cos\varphi + \frac{5}{3\sqrt{3}}\cos\theta\right)^4\right]. \end{aligned} \tag{3}$$

Here the three terms describe the Zeeman energy, the effective uniaxial magnetic anisotropy

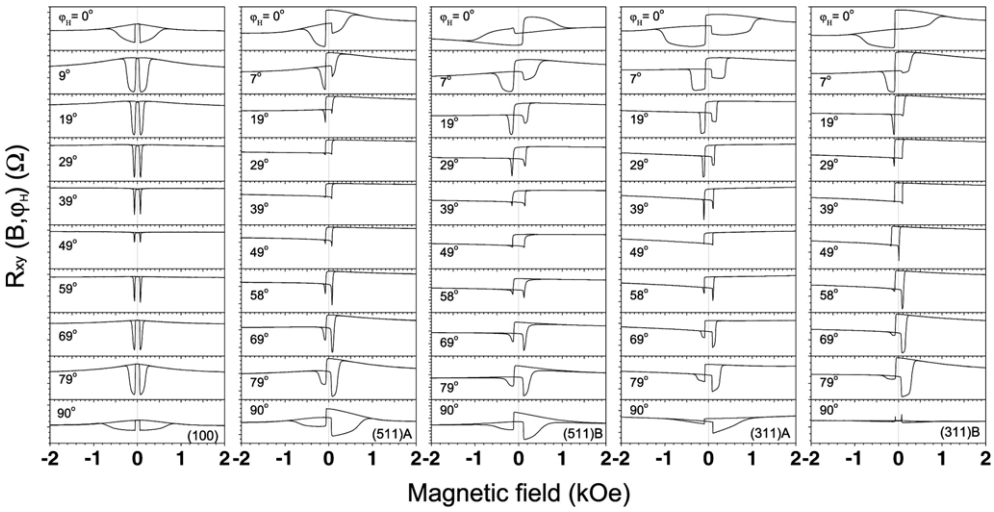

Figure 9. Magnetic field dependence of Hall resistance R_{xy} measured at different applied field angles φ_{H} in the PHE geometry for GaMnAs layers grown on (a) (100), (b) (511)A, (c) (511)B, (d) (311)A, and (e) (311)B substrates.

along the growth direction (the term involving K_{eff}), and the cubic anisotropy, respectively. The angles (θ, φ) and $(\theta_{\mathrm{H}}, \varphi_{\mathrm{H}})$ specify the orientations of magnetization and magnetic field, respectively, and are defined with respect to the coordinates x, y, z, as discussed in section 2. The equilibrium angles of the magnetization (θ, φ) imposed by the minimization of the free energy density for a specific orientation of the applied field $(\theta_{\mathrm{H}}, \varphi_{\mathrm{H}})$ are obtained by solving the equations

$$\begin{aligned} \frac{\partial F}{\partial \varphi} &= 0; \\ \frac{\partial F}{\partial \theta} &= 0. \end{aligned} \tag{4}$$

From (2) or (3), and (4), one can easily derive that the easy axis of magnetization is along one of the $\langle 100 \rangle$ directions when there is no uniaxial anisotropy K_{eff}; and that it tilts slightly toward the growth plane with increasing K_{eff}. However, even in the presence of such tilt, there will exist a finite component of magnetization M_z normal to the sample plane (qualitatively similar, but considerably stronger, than that described for the case of vicinal films in the preceding section). The presence of such M_z is then expected to produce an asymmetry in the value of R_{xy} measured in the PHE geometry, similar to that observed in vicinal GaMnAs layers.

3.2.2. The planar and anomalous Hall effects in high-index-plane GaMnAs films. Figure 9 shows Hall resistances R_{xy} measured in the PHE geometry for GaMnAs grown on (100), (511)A, (511)B, (311)A, and (311)B substrates at various in-plane magnetic field orientations φ_{H} with respect to the current **I**. The field was swept between +2.0 and −2.0 kOe, a +2.0 kOe field being applied prior to each scanning loop to saturate the magnetization of the GaMnAs layer. In all cases seen in figure 9 the in-plane PHE shows a two-step magnetic reversal behaviour, well known in GaMnAs epilayers with easy axes oriented along the [010] and [001] directions, and with the in-plane hard axes along [011] and [01$\bar{1}$].

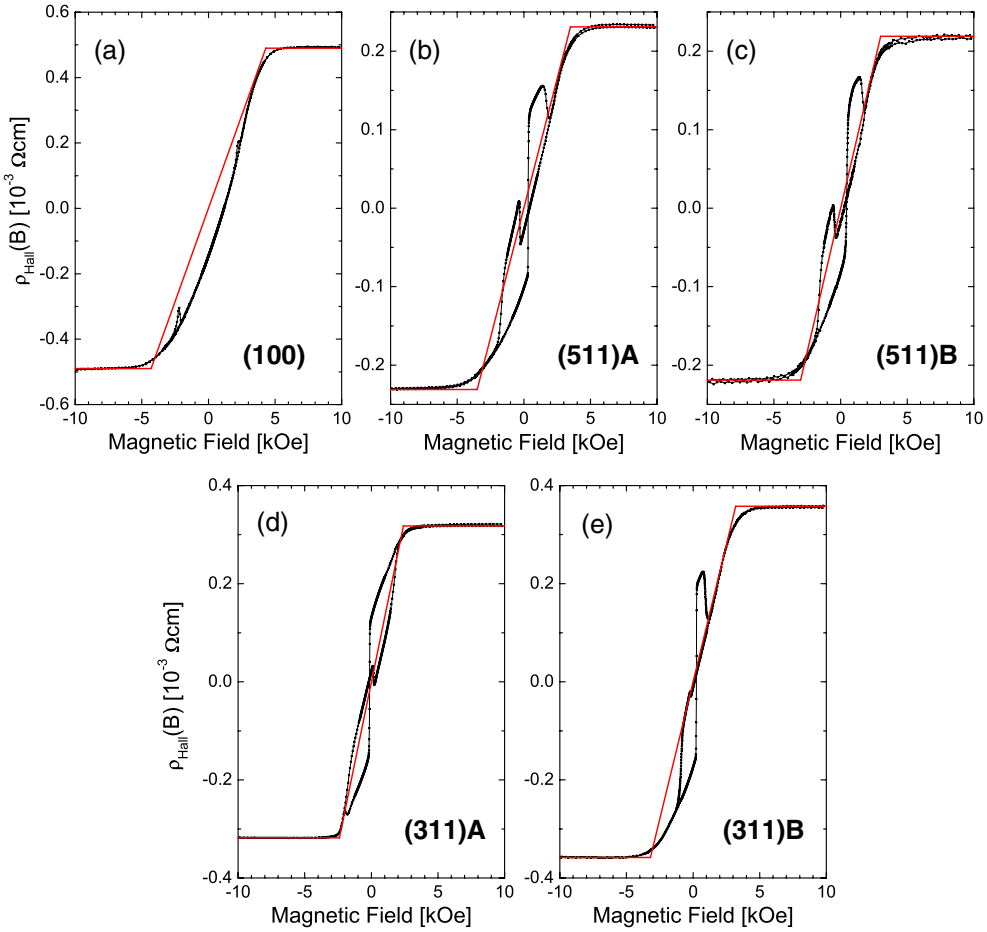

Figure 10. Magnetic field dependence of Hall resistivity $\rho_{xy} = (wd/l)R_{xy}$ observed in the AHE geometry for GaMnAs films grown on (a) (100), (b) (511)A, (c) (511)B, (d) (311)A, and (e) (311)B substrate. The straight red lines are guides for the eye.

We do, however, observe significant differences between R_{xy} obtained on the control sample grown on a (100) substrate and on samples grown on the high-index planes. Specifically, the values of the planar Hall resistance plateaus, representing the intermediate magnetization states in the magnetization reversal, are unequal in samples grown on high-index substrates. As was the case with the vicinal samples discussed in the preceding section, one can also see that in high-index-plane samples there are four distinct resistance states in the hysteresis loops of R_{xy}, depending on the history of the applied fields (i.e., on the sequence of field strengths applied at a given angle).

For completeness, Hall resistivities $\rho_{xy} = R_{xy}\frac{wd}{l}$ (where w is the width of the Hall bar, l is its length, and d is the thickness of the GaMnAs layer) measured at 4.2 K in the AHE geometry are also plotted in figure 10 for the high-index-plane films. We note immediately that the hysteresis loops shown by ρ_{xy} for the high-index-plane GaMnAs layers are much more complicated than those obtained for GaMnAs grown on the (100) substrate. We begin the analysis of the high-index-plane results by examining the ratio of the asymmetric shift of R_{xy} observed at zero field in the PHE geometry to the total AHE resistance change at high fields, in

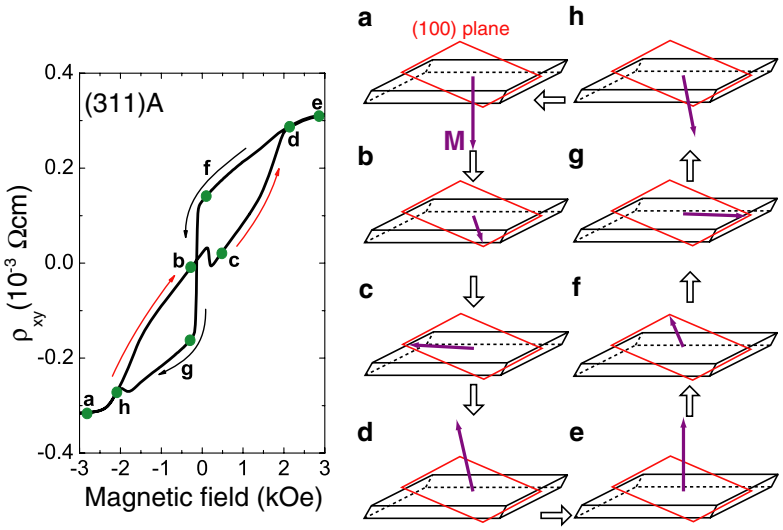

Figure 11. Hall resistivity ρ_{xy} measured in the AHE geometry on GaMnAs grown on a (311)A substrate; and schematic diagrams representing the evolution of magnetization reversal corresponding to the sequence of states from (**a**) to (**h**).

analogy with the ratio $\delta r/\Delta R_{\mathrm{AHE}}$ discussed for vicinal films in figure 4(a). Surprisingly, in the present case the simple linear relation with α is not found, indicating that the simple mechanism invoked in describing vicinal samples cannot quantitatively explain the asymmetric shift in R_{xy} observed in the PHE geometry in high-index-plane samples. Although we still believe that the asymmetric shift of R_{xy} seen in these samples in the PHE geometry originates from the AHE contribution induced by the component of magnetization normal to the sample surface, there are two factors which make the high-index-plane geometry more complicated in the framework of the single-domain assumption. First, as we discussed before, the uniaxial anisotropy K_{eff} will shift the easy axis of magnetization away from either the [010] or the [001] direction toward the growth plane, making the asymmetric shift in R_{xy} smaller than that calculated from (1), the degree of reduction depending on the magnitude of K_{eff}. And second, in the situation where the AHE and PHE contributions become comparable (because of the relatively large value of M_z in high-index-plane samples), the asymmetry of R_{xy} is expected to be particularly pronounced. This is in fact observed in figure 9, for example, for the (311)B sample, where the ratio $\delta r/\Delta R_{\mathrm{AHE}}$ is close to unity. However, unlike in the vicinal case, where we could treat the AHE contribution as a perturbation to PHE, under the present circumstances the AHE and PHE contributions can no longer be simply added linearly together, and one must approach the problem by developing a full conductivity tensor for the high-index-plane geometries, which is beyond the intended scope of this paper.

3.2.3. Magnetization reversal of GaMnAs grown on high-index substrate. We now turn to the details of magnetization reversal in GaMnAs grown on high-index substrates. In the PHE geometry, the process of magnetization reversal is similar to that occurring in GaMnAs grown on vicinal substrate, and we refer the interested reader to a recent paper on the subject by Lim *et al* [11]. In this section we will focus primarily on magnetization reversal observed in the perpendicular (AHE) geometry, i.e., with the magnetic field **H** applied normal to the sample plane.

In figure 11 we show the Hall resistivity $\rho_{xy} = R_{xy}\frac{wd}{l}$ observed at 4.2 K for the GaMnAs layer grown on a (311)A substrate. As shown in figure 1, the longer dimension of the Hall bar sample, and hence the direction of the current **I**, was chosen along the $[\bar{2}33]$ crystallographic direction. The data shown in figure 11 were obtained with the magnetic field **H** normal to the (311) plane (i.e., along z in figure 1). Note that in this geometry the magnetization **M** has components both on the sample plane (the xy plane) and on the normal to that plane (i.e., the z axis). The resulting Hall resistivity ρ_{xy} measured in the AHE geometry thus contains two contributions: one from the 'real' AHE caused by the component of magnetization M_z perpendicular to the sample plane, and one from PHE caused by the component of magnetization on the sample plane. Thus ρ_{xy} measured in a GaMnAs film depends strongly on the relative orientation of the magnetization **M** with respect to the direction of the current **I**.

One should note that all jumps seen in figure 11 are related to domain nucleation and spin switching through an intermediate state [22]. To see this, let us concentrate on the curves and on the corresponding schematic plots in figure 11. In this discussion we will assume that, in the single domain state, the magnetic moment **M** is along one of the easy axes (i.e., along either [010], [001], $[0\bar{1}0]$ or $[00\bar{1}]$ directions) when the applied field is zero. We begin with a large negative field applied in the z direction, where **M** aligns itself along the field direction (i.e., normal to the sample plane), marked as **a** in figure 11. As the field decreases to zero, **M** tilts to the $[0\bar{1}0]$ direction, marked **b** in the figure. Since the AHE and PHE have opposite signs at this point, they tend to cancel, and the resultant value of ρ_{xy} is small. As the magnetic field continues to sweep to a small positive value along z (about 200 Oe), a jump in ρ_{xy} occurs when **M** switches from the $[0\bar{1}0]$ direction (**b**) to [001] (**c**). Note that this jump corresponds to a 90° spin switching in the (100) 'easy' plane, not in the growth plane. With further increase in the field, the direction of **M** continues to tilt further towards the direction of **H**, eventually reaching another change in orientation at 2 kOe that corresponds to a rotation of the magnetization to a direction between [010] and $[\overline{311}]$ direction, marked **d**. As the field continues to increase, **M** turns to align with the applied field, marked **e**.

During the down-sweep, when the field decreases to zero from above, the magnetization **M** rotates to the [010] direction, marked **f**. When the field reaches the value of −200 Oe, a very large jump is observed in ρ_{xy}, corresponding to a 90° domain switching in the (100) plane of **M**, from [010] the $[00\bar{1}]$ direction, marked **g**. Note that at the two states **f** and **g**, the signs of the AHE and PHE resistances are the same (at **f** both are positive, and at **g** both are negative), so that the change of ρ_{xy} during the **f** → **g** switching is much greater than that at the **b** → **c** transition (where the AHE and PHE contribution have opposite signs, thus tending to cancel one another in their combined contribution to ρ_{xy}). As the field continues to decrease toward −2 kOe, the orientation of the magnetic moment **M** approaches that of **H**, and gradually rotates to a direction between [311] and $[0\bar{1}0]$, marked **h**. As the field continues to increase, **M** finally tilts to the field $(-z)$ direction, as shown in the starting position of the cycle marked **a**. Note that this complicated process of magnetization reversal consists of both gradual rotations (e.g., **a** → **b**, **e** → **f**), and rapid spin switchings (e.g., **b** → **c**, **f** → **g**). It is the rapid spin switchings that manifest themselves in the form of the conspicuous abrupt asymmetric 'jumps' in the Hall resistivity ρ_{xy}.

3.2.4. Anisotropic magnetoresistance in high-index-plane GaMnAs layers. It is commonly accepted that PHE in ferromagnetic semiconductors such as GaMnAs is a combined result of anisotropic magnetoresistance (AMR) and strong spin–orbit coupling. For completeness, in this section we will therefore present experimental AMR results obtained on GaMnAs grown on high-index planes, and measured using an in-plane magnetic field **H** = 10 kOe. In figure 12, the results of $\Delta R/R_{\|}$ obtained in this study are plotted in the form of a polar diagram, where

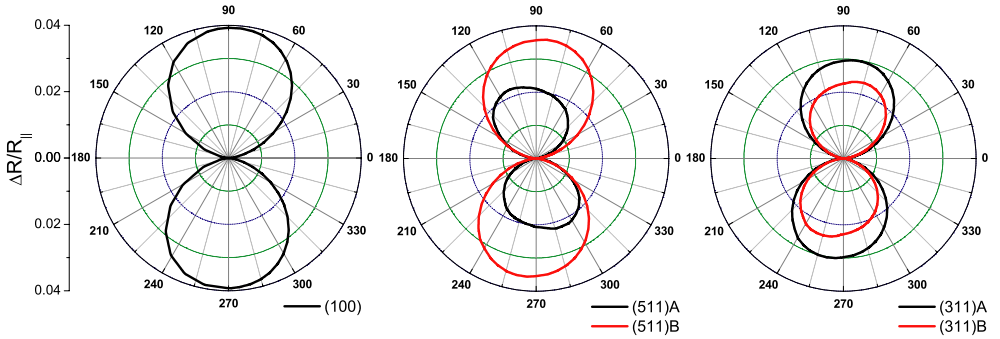

Figure 12. Polar diagrams of $\Delta R/R_{\parallel}$ obtained from measurements of AMR on GaMnAs layers grown on different substrates.

$\Delta R(\varphi_{\mathrm{H}}) = [R_{xx}(\varphi_{\mathrm{H}}) - R_{\parallel}]/R_{\parallel}$, $R_{xx}(\varphi_{\mathrm{H}})$ is the resistance measured with **H** applied at an angle φ_{H} with respect to the current **I** in the sample plane, and $R_{\parallel}$ is the resistance measured with **H** parallel to **I**, i.e., along [011], [$\bar{2}$33], or [$\bar{2}$55] for samples grown on the (100), (311), or (511) planes, respectively. As shown in figure 12, in GaMnAs grown on a (100) substrate, the angular profiles follow roughly a $\sin^2(\varphi_{\mathrm{H}})$ law [23, 24], the maxima of $R(\varphi_{\mathrm{H}})$ occurring for **H** normal to the current **I** (i.e., $\varphi_{\mathrm{H}} = 90°$ and 270°), and the minima for **H** parallel or antiparallel to the current **I** (i.e., $\varphi_{\mathrm{H}} = 0°$ and 180°). Surprisingly, in GaMnAs grown on high-index substrates, although the basic angular profile of $\Delta R(\varphi_{\mathrm{H}})$ is similar to that observed on the 'standard' (100) GaMnAs, the maximum of $R(\varphi_{\mathrm{H}})$ does not occur at **H** normal to the current **I**. However, in our experimental results on the four high-index-plane GaMnAs layers this small deviation does not appear to follow any systematic pattern. While we cannot present a meaningful explanation for this new phenomenon based on the limited data now available, we feel that this abnormal AMR behaviour in high-index samples merits further exploration, since it may shed additional light on the processes that govern AMR (and thus also PHE) in GaMnAs and in related III–Mn–V alloys.

4. Summary

We have successfully grown GaMnAs epilayers on tilted and high-index GaAs substrates. Measurements in the PHE and AHE geometries on these samples reveal that the orientation of the easy axis of magnetization in GaMnAs films does not originate from the shape of the specimen (shape anisotropy), magnetocrystalline anisotropy being the dominant mechanism which determines the direction of the easy axis. The Hall resistance R_{xy} measured in these samples in the PHE geometry shows a characteristic asymmetry as a function of the applied field, that contrasts sharply with R_{xy} measured in the same geometry on (100)-grown GaMnAs films. We have demonstrated that the above asymmetry arises from a contribution of the AHE caused by a small but finite component of magnetization **M** normal to the surface of the sample. This component is present because **M** is constrained to the easy (100) plane (usually to directions along [001] or [010]), that in such 'tilted' film orientations is not coincident with the layer plane. We also note that the temperature dependence of R_{xy} in vicinal GaMnAs samples is additionally complicated due to the easy axis switching from the [001] or [010] directions to the [0$\bar{1}$1] orientation as the temperature is increased.

The behaviour of the asymmetry in R_{xy} reported in this paper is especially interesting in that in samples with finite vicinal angle the values of R_{xy} observed in the PHE geometry

show four residual resistance states that depend on the history of how the field was applied before it was switched off. This is in contrast to the PHE observed in non-tilted samples, which shows only two residual states in R_{xy}. Using the above fourfold 'memory' present in the Hall resistance R_{xy}, we were able to demonstrate a prototype four-state MRAM memory device achieved by applying two magnetic fields in different sequences before the field is switched off.

As noted above, the asymmetry in R_{xy} represents the combined effect of PHE and AHE. The ability to investigate effects of PHE and AHE contributing simultaneously to the same measured quantity in a series of samples provided the opportunity to discover that the two effects are functionally related. The fact that such a relation exists is quite surprising, because the AHE is generally ascribed to processes different from those determining the PHE (the AHE is usually discussed in terms of skew or side-jump scattering of carriers, while the PHE in GaMnAs is described in terms of AMR). Although we do not understand the connection between the PHE and AHE reported in this paper, this observation points to the possibility that the two effects are fundamentally related. We therefore feel that this observation provides important new input into the picture of magnetotransport in ferromagnetic semiconductors, and should be followed by further experimental as well as theoretical exploration.

Furthermore, our analysis of R_{xy} in high-index GaMnAs measured in the AHE geometry (i.e., with the applied field **H** normal to the sample plane) indicates that the multistep magnetization jumps accompanying the reversal of magnetization originate from irreversible noncoherent spin switching that results from domain nucleation and expansion. In our experiments we find that in high-index-plane GaMnAs films such irreversible noncoherent spin switching occurs at the (100) plane rather than in the growth plane, resulting in highly complex hysteresis loops observed in R_{xy} in the AHE geometry. Finally, we observe abnormal AMR in GaMnAs films grown on high-index substrates, indicating that in such 'tilted-plane' films the maximum of magnetoresistance does not occur when **H** is normal to the current **I**, but at some non-orthogonal **H** versus **I** orientation. Further detailed investigation of this phenomenon should be especially informative, in that it can shed additional light on the AMR, PHE and AHE in GaMnAs and in related III–Mn–V ferromagnetic semiconductors.

Acknowledgments

This work was supported by the NSF Grant DMR06-03752 and NSF-NIRT Program DMR02-10519.

References

[1] Ohno H 1998 *Science* **281** 951
[2] Ohno H 1999 *J. Magn. Magn. Mater.* **200** 110
[3] Dietl T, Ohno H and Matsukura F 2001 *Phys. Rev.* B **63** 195205
[4] Furdyna J K, Liu X, Lim W L, Sasaki Y, Wojtowicz T, Kuryliszyn I, Lee S, Yu K M and Walukiewicz W 2003 *J. Korean Phys. Soc.* **42** S579
[5] Liu X and Furdyna J K 2006 *J. Phys.: Condens. Matter* **18** R245
[6] Omiya T, Matsukura F, Shen A, Ohno Y and Ohno H 2001 *Physica* E **10** 206
[7] Wang K Y, Edmonds K W, Zhao L X, Sawicki M, Campion R P, Gallagher B L and Foxon C T 2005 *Phys. Rev.* B **72** 115207
[8] Daeubler J, Glunk M, Schoch W, Limmer W and Sauer R 2006 *Appl. Phys. Lett.* **88** 051904
[9] Pross A, Bending S J, Wang K Y, Edmonds K W, Campion R P, Foxon C T, Gallagher B L and Sawicki M 2006 *J. Appl. Phys.* **99** 093908
[10] Lim W L, Liu X, Dziatkowski K, Ge Z, Shen S, Furdyna J K and Dobrowolska M 2006 *J. Appl. Phys.* **99** 08D505
[11] Lim W L, Liu X, Dziatkowski K, Ge Z, Shen S, Furdyna J K and Dobrowolska M 2006 *Phys. Rev.* B **74** 045303

[12] Reinwald M, Wurstbauer U, Döppe M, Kipferl W, Wagenhuber K, Tranitz H P, Weiss D and Wegscheider W 2005 *J. Cryst. Growth* **278** 690
[13] Wolf S A, Awschalom D D, Buhrman R A, Daughton J M, von Molnár S, Roukes M L, Chtchelkanova A Y and Treger D M 2001 *Science* **294** 1488
[14] Bihler C, Huebl H, Brandt M S, Goennenwein S T B, Reinwald M, Wurstbauer U, Döppe M, Weiss D and Wegscheider W 2006 *Appl. Phys. Lett.* **89** 012507
[15] Hurd C M 1980 *The Hall Effect and Its Applications* ed C L Chien and C R Westgate (New York: Plenum) p 3
[16] Tang H X, Kawakami R K, Awschalom D D and Roukes M L 2003 *Phys. Rev. Lett.* **90** 107201
[17] Welp U, Vlasko-Vlasov V K, Liu X, Furdyna J K and Wojtowicz T 2003 *Phys. Rev. Lett.* **90** 167206
[18] Sawicki M, Matsukura F, Idziaszek A, Dietl T, Schott G M, Ruester C, Gould C, Karczewski G, Schmidt G and Molenkamp L W 2004 *Phys. Rev.* B **70** 245325
[19] Hamaya K, Taniyama T, Kitamoto Y, Fujii T and Yamazaki Y 2005 *Phys. Rev. Lett.* **94** 147203
[20] Sawicki M, Wang K Y, Edmonds K W, Campion R P, Staddon C R, Farley N R S, Foxon C T, Papis E, Kamińska E, Piotrowska A, Dietl T and Gallagher B L 2005 *Phys. Rev.* B **71** 121302(R)
[21] Pampuch C, Das A K, Ney A, Daweritz L, Koch R and Ploog K H 2003 *Phys. Rev. Lett.* **91** 147203
[22] Liu X, Lim W L, Titova L V, Dobrowolska M, Furdyna J K, Kutrowski M and Wojtowicz T 2005 *J. Appl. Phys.* **98** 63904
[23] Weiss H 1966 *Semiconductors and Semimetals* vol 1, ed R K Willardson and A C Beer (New York: Academic) and references therein
[24] Weiss H and Wilhelm M 1963 *Z. Phys.* **176** 399